

MODELLING KAON ELECTROPRODUCTION ON PROTONS AND LIGHT  
NUCLEI

TATIANA ANGELESCU, OLIVER K. BAKER<sup>a</sup>, ALEXANDRU MIHUL, GABRIEL  
NICULESCU<sup>a</sup>, IOANA NICULESCU<sup>a</sup> and LILIANA TEODORESCU

*Faculty of Physics, Bucharest University, PO Box Mg12, Romania*  
*<sup>a</sup>Hampton University, Hampton, VA 23668, U.S.A.*

Received 24 January 1996

UDC 539.17.02

PACS 25.80.Nv

The Continuous Electron Beam Accelerator Facility (CEBAF) is by its high current and precision an excellent tool in studying hadronic structure. The experiment approved for 1996 aims at the separation of the longitudinal and transverse cross-sections and the  $K^+$  form-factor measurement in the reaction  $p(e, e' K^+) \Lambda/\Sigma$ . Kinematic conditions and trigger modelling have been computed for the two-arm spectrometer with a programme which optimizes the experimental conditions taking into account the expected cross-section and the spectrometer acceptance.

### 1. Introduction

Electroproduction is an efficient tool for studying particle structure. Quantum electrodynamics has been proved to be valid for leptons up to a very high order, and electromagnetic interaction can be treated in the one-photon approximation (OPA) due to the small value of the coupling constant  $\alpha$ .

Using these well established assumptions, we can write the differential cross-section for scattering of unpolarized electrons in an unpolarized target [1]. It has four components which can be separated using suitable experimental configurations:

$$\frac{d\sigma}{dt} = \sigma_U + \epsilon\sigma_L + \epsilon \cos(2\phi) \sigma_{TT} + \left[ \frac{\epsilon(\epsilon + 1)}{2} \right]^{1/2} \cos \phi \sigma_{LT} \quad (1)$$

where  $\phi$  is the angle between the scattering and production planes,  $t$  is the four-momentum transfer from the virtual photon to the kaon and  $\epsilon$  is the polarization of the virtual photon.

The kaon cross-section components are related to the virtual photon helicity amplitudes:

1.  $\sigma_U$  is the cross-section for transverse unpolarized virtual photons and can be compared with unpolarized real photon cross-section for very small four-momentum transfer values.
2.  $\sigma_L$  is the cross-section for longitudinally polarized photons and is an attribute of the virtual photons only. The longitudinal virtual photons having zero helicity are able to produce pions or kaons moving along their direction. If dominated by the kaon-pole contribution,  $\sigma_L$  can provide a value of the kaon form-factor by using the Chew-Low extrapolation method.
3.  $\sigma_{TT}$  describes the modification in the cross-section if the transverse photons are partially polarized.
4.  $\sigma_{LT}$  is the result of the interference between longitudinal and transverse components.

For zero four-momentum transfer, i.e. for real photons,  $\epsilon$  vanishes and the virtual cross-section becomes the photoproduction cross-section.

The separation of the four components of the cross-section can provide valuable information about the photoproduction with real and virtual photons. The advantage of the virtual-photon reaction is the fact that the polarization is precisely known and can be varied in large limits by choosing different kinematical configuration. The separation of the four cross-sections does not involve model-dependent methods. This is the most important advantage of the experiment proposed at CEBAF by our group and described in Ref. 2.

This paper presents a programme performing the kinematical computations, the counting rate and trigger efficiency evaluations depending on the experimental possibilities of the project in reaching the proposed goal. The program takes into account the two-arm spectrometer acceptances, neglecting multiple scattering and detector resolution. A Monte-Carlo simulation of the missing mass distribution in kaon electroproduction on deuterium shows the possible degree of  $\Lambda/\Sigma$  separation due to the Fermi motion inside the deuterium nucleus.

The cross-sections used in counting rate evaluations were based on the previous experimental data obtained by other groups and extrapolated for our kinematic configurations. We did not use theoretical predictions for the cross-sections because

many models involve parameters (coupling constants, form-factors) obtained by the authors using the same experimental data.

The program can be used for computing background diagram contributions. For  $\Lambda$  and  $\Sigma$  channels separation, the missing mass distribution can be modelled taking into account radiative corrections or spectator distributions in other light nuclei.

## *2. Modelling two-arm spectrometer for $K^+$ electroproduction*

The study of kaon electroproduction on protons and deuterons at CEBAF HMS-SOS facility benefits from some characteristic which lead to much more complete and reliable results than those obtained in the previous experiments [3-5]:

1. The first and most important new contribution of the experiment should be the separation of the transverse and longitudinal cross-section by varying the polarization  $\epsilon$  in a large range ( $0.28 \leq \epsilon \leq 0.86$ ) in the same experiment.
2. The electron-four momentum transfer  $Q^2$  range extends from  $0.5 \text{ (GeV/c)}^2$  up to  $2.0 \text{ (GeV/c)}^2$ . Using the Chew-Low extrapolation technique for the longitudinal cross-section, one should be able obtain a  $Q^2$  dependence of the kaon form-factor for a large range and thus test different theoretical predictions.
3. The ratio of the cross-section for  $K^+\Lambda$  and  $K^+\Sigma^0$  channels in the Bjorken variable range  $0.2 \leq x \leq 0.5$  could give an answer about the strangeness content of the proton as predicted by Nachtmann [6].
4. The measurement of the out of plane kaon electroproduction for  $-10^\circ \leq \phi \leq 10^\circ$ , with a precision of  $0.06^\circ$ , would lead to the separation of  $\sigma_{LT}$  and  $\sigma_{TT}$  for  $t$  in the range 0.11 to  $0.50 \text{ (GeV/c)}^2$ .
5. The uncertainty of kinematic parameter values is expected to be about 1% and the uncertainty on the cross-section less than 5%. In this way the errors of the separated cross-sections are smaller than those obtained in previous experiments.

### *2.1. Phase-space limitations for the CEBAF two-arm spectrometer*

The limitations imposed by the experimental conditions define the range of variation for the variables:  $Q^2$ ,  $W$ ,  $t$ ,  $\epsilon$ . The proposal [2] gives the experimental conditions which define the kinematical limits:

1. The scattered electron angle can vary from  $14.5^\circ$  to  $61.4^\circ$ .
2. The produced kaon can be detected between  $13.5^\circ$  and  $23.6^\circ$ .

3. The electron momentum can be varied between 0.7 and 2.4 GeV/c with a 20% acceptance.
4. The kaon momentum can be varied between 1.0 and 1.7 GeV/c with a 40% acceptance.

The  $K^+$  electroproduction starts with a threshold value for the invariant mass of the  $K\Lambda$  system,  $W$ :

$$W_{min} = m_{\Lambda} + m_K = 1.61 \text{ GeV}. \quad (2)$$

This limitation will fix the minimum energy of the virtual photon  $\nu$ :

$$\nu_{min} = \frac{W_{min}^2 + Q^2 - M^2}{2M}, \quad (3)$$

where  $M$  is the proton mass.

The  $Q^2$  value is limited by the electron scattering angle and the beam energy. The minimum scattering angle ( $14.5^\circ$ ) leads to the minimum  $Q^2$  value

$$Q_{min}^2 = E_e(E_e - \nu) \sin^2(\theta_{min}/2), \quad (4)$$

where  $E_e$  is the beam energy.

The minimum four-momentum transfer from the virtual photon to the kaon,  $t_{min}$ , depends on  $W$ ,  $Q^2$  and  $E_e$ . Its dependence on  $Q^2$  and the kaon momentum  $p_K$  for  $W = 1.84$  GeV and  $E_e = 4$  GeV is given in Fig. 1. The Chew-Low extrapolation of the longitudinal cross-section depends on the minimum four-momentum transfer  $t_{min}$ . In order to obtain smaller  $t_{min}$  values, we need higher  $W$  values. Especially for high  $Q^2$ ,  $W$  is limited by the angular range of the kaon-arm spectrometer.

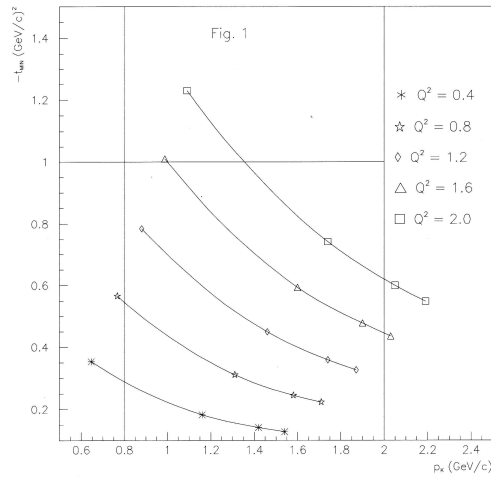


Fig. 1. Dependence of  $t_{min}$  on kaon laboratory momentum for different  $Q^2$  values.

To obtain high  $Q^2$  values, we are constrained to work near the threshold ( $W \approx 1.7$  GeV) for small beam energy.

The Bjorken variable  $x$  is limited to a short-range of values,  $0.2 \leq x \leq 0.5$ , not interesting for deep inelastic scattering studies. However, measurements of the  $K\Lambda$  and  $K\Sigma^0$  cross-sections with high precision extend the possibility to check the strangeness content of the proton given by the theoretical models [6].

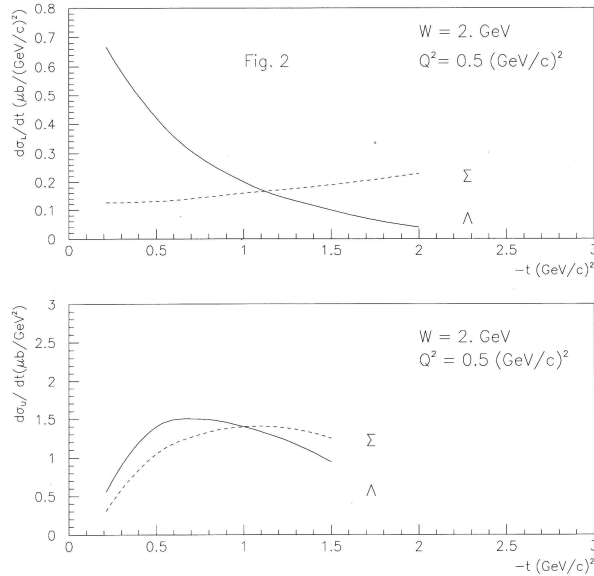


Fig. 2. Dependence of  $\sigma_U$  and  $\sigma_L$  on  $t$  according to Williams and Cotanch model [7].

As one of the most important goals of this experiment is the transverse/longitudinal cross-section separation. We show in Fig. 2 the dependence of  $\sigma_U$ ,  $\sigma_L$  on  $t$  and a set of measurements proposed in this experiment.

## 2.2. Kaon electroproduction cross-sections

Table 1 gives the kinematical settings chosen in the experiment for the transverse longitudinal cross-section separation in the kaon electroproduction on nucleon:

$$e + p \rightarrow e' + K^+ + \Lambda(\Sigma^0), \quad (5)$$

$$e + n \rightarrow e' + K^+ + \Sigma^-. \quad (6)$$

At these values for  $W$ , all other strange particle production channels are closed (for example  $K^+K^-N$ ). The pion rejection achieved will be  $10^3$  using time-of-flight and Cherenkov counter in the kaon-arm spectrometer (SOS) [2]. In the electron

spectrometer arm (HMS) the pion rejection will be about 500. Therefore, the background in the two-arm coincidence experiment will be due to the reactions (aa) and (aaa) with different kinematical configurations accepted by the spectrometer during the resolution time of the coincidence scheme.

TABLE 1.  
Kinematical configurations for cross-section  $t$  dependence.

| Kine. | $Q^2$<br>(GeV/c) <sup>2</sup> | $E_e$<br>GeV | $E'_e$<br>GeV | $\theta_e$<br>deg. | $\theta_\gamma$<br>deg. | $W$<br>GeV | $p_K$<br>GeV/c | $\epsilon$ | $t$<br>(GeV/c) <sup>2</sup> |
|-------|-------------------------------|--------------|---------------|--------------------|-------------------------|------------|----------------|------------|-----------------------------|
| t1b   | 0.65                          | 3.5          | 1.70          | 19.03              | 16.31                   | 1.90       | 1.40           | 0.75       | 0.228                       |
| t2b   | 0.50                          | 3.5          | 1.70          | 16.68              | 14.57                   | 1.94       | 1.43           | 0.75       | 0.169                       |
| t3b   | 0.35                          | 3.5          | 1.69          | 13.96              | 12.41                   | 1.98       | 1.46           | 0.76       | 0.121                       |
| t4b   | 0.75                          | 3.5          | 1.46          | 22.10              | 14.33                   | 1.99       | 1.66           | 0.67       | 0.214                       |

Counting rate evaluation in the two-spectrometer arm should start with the kaon cross-sections of the reaction investigated. We chose as input the data obtained by Bebek [4], as the most recent and reliable.  $d\sigma^{CMS}/d\Omega_K$  has been extrapolated to the kinematical settings used in our experiment ( $W$ ,  $Q^2$ ,  $t$ ), by using the extrapolation law [4]:

$$\frac{W(W^2 - M^2)(Q^2 + a)}{p_K^{CMS} e^{2.1t}} \frac{d\sigma^{CMS}}{d\Omega_K} = \text{const.}, \quad (7)$$

with  $a = 2.67$  for  $\Lambda$  production, and  $a = 0.79$  for  $\Sigma^0$  production.

For evaluating the counting rate we used the following cross-sections:

### 2.2.1. Kaon electroproduction cross-section

The laboratory system cross-section for reactions (5) and (6) is given by:

$$\sigma(e, e', K) = \frac{d^3\sigma}{dE'_e d\Omega_e d\Omega_K} = \Gamma \frac{d\sigma^{CMS}}{d\Omega_K} \frac{d(\cos\theta^{CMS})}{d(\cos\theta)}, \quad (8)$$

where

$$\Gamma = \frac{\alpha/4\pi^2 E'(W^2 - M^2)}{EMQ^2(1 - \epsilon)} \quad (9)$$

is the virtual photon flux, and  $d\sigma^{CMS}/d\Omega_K$  is the extrapolated cross-section according to Ref. 4. In computing the cross-section for reaction (6), we made the assumption:

$$\sigma(\gamma_n \Rightarrow K^+ \Sigma^-) = \sigma(\gamma_p \Rightarrow K^+ \Sigma^0), \quad (10)$$

which is supported by the experimental data of Bebek [4].

The cross-section given by Eq. (8) was used to evaluate the coincidence counting rate.

### 2.2.2. Cross-section for elastic electron scattering on nucleon

The elastic electron scattering on nucleons has been computed using the relation [8]:

$$\sigma(e, e') = \frac{d\sigma}{d\Omega_e} = \sigma_{\text{Mott}} \left( \frac{G_E^2 + \frac{Q^2}{4M^2} G_M^2}{1 + \frac{Q^2}{4M^2}} + \frac{Q^2}{2M^2} G_M^2 \tan^2(\theta/2) \right), \quad (11)$$

where  $G_E$  and  $G_M$  are the elastic and magnetic form-factors of the target (proton or neutron) and  $\sigma_{\text{Mott}}$  is the Mott cross-section:

$$\sigma_{\text{Mott}} = \frac{\alpha^2 \cos^2 \theta/2}{4E_e^2 \sin^4 \theta/2} \frac{E_e'}{E_e}. \quad (12)$$

The cross-section computed with the relation (11) has been used in evaluating electron-arm counting rate and consequently the background coincidence events.

### 2.2.3. Kaon-arm integrated cross-section

We integrated the  $(e, e', K)$  cross-section expressed as a function of  $W$  and  $Q^2$  for all  $K^+$  momentum values accepted by the kaon-arm spectrometer at a given angle:

$$\sigma(e, K) = \int dW^2 \int \Gamma' \frac{d\sigma^{CMS}}{d\Omega_K} \frac{d(\cos \theta^{CMS})}{d(\cos \theta)} dQ^2, \quad (13)$$

where

$$\Gamma' = \frac{\alpha}{16\pi^2} \frac{W^2 - M^2}{E^2} \frac{1}{M^2 Q^2 (1 - \epsilon)}, \quad (14)$$

$$W_{\min} = M_A + M_K, \quad (15)$$

$$W_{\max} = s^{1/2} - M_e, \quad (16)$$

$$Q_{\min}^2 = 0, \quad (17)$$

and

$$Q_{\max}^2 = 4(E_e E_e')^{GSMS}. \quad (18)$$

GSMS is the general center of mass  $(e, N)$  system.

This integrated cross-section will give the counting rate in the kaon arm for accidental coincidences.

### 2.3. Counting rates

#### 2.3.1. Coincidence counting rate

This counting rate is determined by true coincidence between the scattered electron and the  $K^+$  in reactions (5) and (6). We evaluated it using the  $\sigma(e, e', K^+)$  given by (ab).

The coincidence rate is:

$$R_c = \sigma(e, e', K^+) \exp(-Lm_K/p_K\tau_K)\Delta E_e\Delta\Omega_e\Delta\Omega_K n_e n_t t, \quad (19)$$

where,  $n_e = I/q_e$ ,  $I$  is the beam intensity,  $n_t$  the density of nuclei in the target,  $t$  the target length,  $\Delta E_e$  the energy acceptance in the electron-arm,  $\Delta\Omega_e$  the angular acceptance in the electron-arm and  $\Delta\Omega_K$  is the angular acceptance in the kaon-arm.

The exponential term define the probability that the kaon does not decay before detection.

#### 2.3.2. Electron-arm counting rate

The electron-arm counting rate is evaluated using the elastic electron scattering cross-section given by Eq. (8). It has been computed separately for protons and neutrons according to the relation:

$$R_e = \frac{d\sigma}{d\Omega_e} n_e n_t t \Delta\Omega_e. \quad (20)$$

#### 2.3.3. Kaon-arm counting rate

The kaon-arm counting rate has been evaluated according to the procedure described in (2.2.3) with  $\sigma(e, K)$  given by Eq. (13):

$$R_K = \sigma(e, K^+) \exp(-LM_K/p_K\tau_K)\Delta\Omega_K n_e n_t t. \quad (21)$$

Using these rates, we computed the ratio of accident and true events for a given resolution time ( $\tau_{res}$ ) in the coincidence scheme:

$$\frac{A}{T} = \frac{\tau_{res} R_e R_K}{f R_c}. \quad (22)$$

$f$  is the duty factor ( $f = 1$  for CEBAF). The ratio  $A/T$  is an important characteristic of the experiment: it defines the efficiency of the triggering system.

## 3. Results and facilities of the program

The program for the computation of kinematics, cross-sections and counting rates starts with the reactions (5) and (6) and combines the cross-section data



to obtain rates for reactions on nuclei without taking into account the nuclear interaction

$$e + {}^A_Z\text{N} \rightarrow e' + \text{K}^+ + X. \quad (23)$$

We applied the model for deuterium where the binding energy is small. Table 2 shows the computed rates for the kinematical settings shown in Table 1 for deuterium electroproduction. It is seen that, except for small  $Q^2$  values where  $A/T$  is still high, we can reduce the accidental events to less than 10%.

TABLE 2.  
Counting rates for cross-section  $t$  dependence.

| Kine. | $I$<br>( $\mu\text{A}$ ) | $R_c(e, e', \text{K})$<br>$\text{s}^{-1}$ | $R_e(e, e')$<br>$10^3 \text{ s}^{-1}$ | $R_K(e, \text{K})$<br>$10^3 \text{ s}^{-1}$ | $A/T$<br>$\tau_{\text{rez}} = 2 \text{ ns}$ |
|-------|--------------------------|-------------------------------------------|---------------------------------------|---------------------------------------------|---------------------------------------------|
| t1b   | 30                       | 0.693                                     | 19.60                                 | 0.739                                       | 0.042                                       |
| t2b   | 30                       | 1.126                                     | 48.99                                 | 0.821                                       | 0.070                                       |
| t3b   | 30                       | 1.970                                     | 153.75                                | 0.910                                       | 0.142                                       |
| t4b   | 30                       | 0.430                                     | 8.30                                  | 0.919                                       | 0.035                                       |

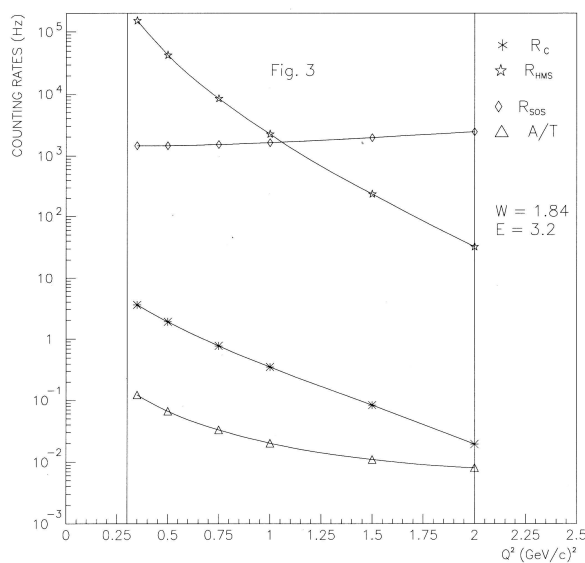


Fig. 3. Dependence of counting rates on  $Q^2$  for  $W = 1.84 \text{ GeV}$  and  $E_e = 3.2 \text{ GeV}$ .

Using the computed values of the coincidence counting rate and the accidental on true events ratio, we can optimize the experimental conditions with respect to the kinematical variables. As an example, we show in Fig. 3 the dependence of the rates on  $Q^2$  for  $W = 1.84 \text{ GeV}$  at the beam energy of  $3.2 \text{ GeV}$ . Figure 4 shows the rate dependence on  $W$  for the same beam energy and for  $Q^2 = 2.0 \text{ (GeV/c)}^2$ . We

can see a steep decrease of the coincidence rate with  $Q^2$ , as expected. The ratio  $A/T$  does not vary very much with  $W$  and is flat beyond  $W = 1.7$  GeV. According to this behaviour, the kinematic configurations in the experiment have been chosen at about the same value of  $W$  (1.84 GeV), for  $Q^2$  as large as possible. For higher energies, the kinematics would permit better separation in  $\epsilon$ .

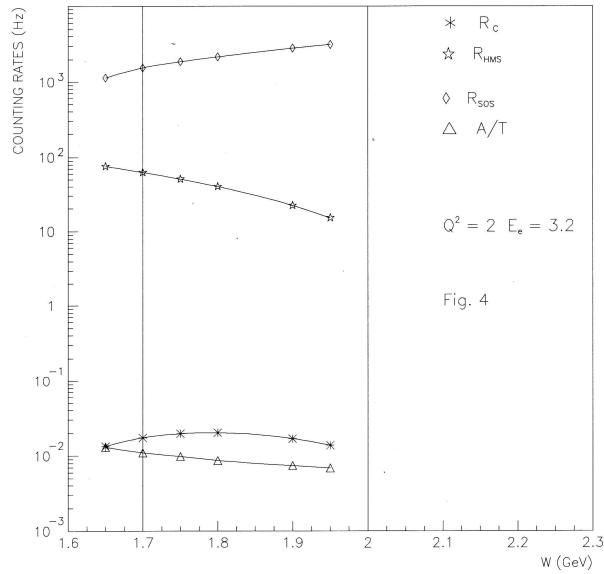


Fig. 4. Dependence of counting rates on  $W$  for  $Q^2 = 2$  (GeV/c) $^2$  and  $E_e = 3.2$  GeV.

TABLE 3.  
Kinematical settings for the  $d(e, e' K^+) \Lambda, \Sigma^0, \Sigma^-$  experiment.

| Kine. | $Q^2$<br>(GeV/c) $^2$ | $E_e$<br>GeV | $E'_e$<br>GeV | $\theta_e$<br>deg. | $\theta_\gamma$<br>deg. | $W$<br>GeV | $\nu$<br>GeV | $\epsilon$ | $x$  |
|-------|-----------------------|--------------|---------------|--------------------|-------------------------|------------|--------------|------------|------|
| 1.a   | 0.50                  | 2.40         | 0.80          | 29.56              | 13.04                   | 1.84       | 1.60         | 0.54       | 0.17 |
| 1.b   | 0.50                  | 3.20         | 1.57          | 18.25              | 16.31                   | 1.84       | 1.60         | 0.76       | 0.17 |
| 1.c   | 0.50                  | 4.00         | 2.39          | 13.16              | 18.10                   | 1.84       | 1.60         | 0.86       | 0.17 |
| 2.a   | 1.00                  | 2.40         | 0.61          | 49.20              | 12.76                   | 1.81       | 1.80         | 0.36       | 0.30 |
| 2.b   | 1.00                  | 3.20         | 1.38          | 27.69              | 18.08                   | 1.81       | 1.80         | 0.66       | 0.30 |
| 2.c   | 1.00                  | 4.00         | 2.19          | 19.48              | 20.77                   | 1.81       | 1.80         | 0.80       | 0.30 |
| 3.a   | 1.50                  | 2.40         | 0.61          | 61.37              | 12.98                   | 1.69       | 1.85         | 0.28       | 0.43 |
| 3.b   | 1.50                  | 3.20         | 1.34          | 34.39              | 19.91                   | 1.69       | 1.85         | 0.61       | 0.43 |
| 3.c   | 1.50                  | 4.00         | 2.23          | 23.42              | 23.56                   | 1.69       | 1.85         | 0.78       | 0.43 |
| 4.a   | 2.00                  | 3.20         | 0.79          | 53.14              | 13.03                   | 1.69       | 1.84         | 0.34       | 0.44 |
| 4.b   | 2.00                  | 3.50         | 1.09          | 42.51              | 15.33                   | 1.69       | 1.84         | 0.46       | 0.44 |
| 4.c   | 2.00                  | 4.00         | 1.59          | 32.67              | 17.90                   | 1.69       | 1.84         | 0.60       | 0.44 |

TABLE 4.  
Coincidence and single rates for the  $d(e, e' K^+) \Lambda, \Sigma^0, \Sigma^-$  experiment.

| Kine. | $I$<br>( $\mu\text{A}$ ) | $R_c(e, e', K)$<br>$10^{-2} \text{ s}^{-1}$ | $R_e(e, e')$<br>$10^3 \text{ s}^{-1}$ | $R_K(e, K)$<br>$10^3 \text{ s}^{-1}$ | $A/T$<br>(ns) |
|-------|--------------------------|---------------------------------------------|---------------------------------------|--------------------------------------|---------------|
| 1.a   | 10                       | 6.50                                        | 5.30                                  | 1.33                                 | 0.11          |
| 1.b   | 10                       | 19.1                                        | 24.0                                  | 1.22                                 | 0.15          |
| 1.c   | 10                       | 38.0                                        | 56.5                                  | 1.19                                 | 0.17          |
| 2.a   | 20                       | 2.14                                        | 0.40                                  | 3.32                                 | 0.06          |
| 2.b   | 20                       | 7.20                                        | 2.78                                  | 2.70                                 | 0.10          |
| 2.c   | 20                       | 15.4                                        | 7.50                                  | 2.10                                 | 0.12          |
| 3.a   | 30                       | 0.56                                        | 0.09                                  | 2.34                                 | 0.04          |
| 3.b   | 30                       | 1.94                                        | 0.70                                  | 1.90                                 | 0.07          |
| 3.c   | 30                       | 4.10                                        | 1.97                                  | 1.70                                 | 0.08          |
| 4.a   | 30                       | 0.94                                        | 0.06                                  | 8.52                                 | 0.05          |
| 4.b   | 30                       | 1.44                                        | 0.12                                  | 7.45                                 | 0.06          |
| 4.c   | 30                       | 2.47                                        | 0.28                                  | 6.36                                 | 0.07          |

#### 4. Conclusions

Preliminary computations for the experimental study of kaon electroproduction have been performed in order to optimize the kinematical set-ups and evaluate the countings rates, statistical errors, background contributions and the running time for each set-up. The program has been used in run-plan evaluations for the experiment accepted to be performed at CEBAF in 1996 [2].

#### References

- 1) J. Martino, *An Introduction to Electron-Scattering Hadronic Physics with MultiGeV Electrons*, Les Houches 6-15 Febr. 1990, New York 1991;
- 2) O. K. Baker et al., *Longitudinal/Transverse Cross-Section Separation in  $p(e, e', K)\Lambda(\Sigma)$  for  $0.5 \leq Q^2 \leq 2.0 \text{ (GeV/c)}^2$* , CEBAF Proposal E 93-018, 1993;
- 3) G. N. Brown et al., *Phys. Rev. Lett.* **28** (1972) 1086;
- 4) C. J. Bebek, C. N. Brown, P. Bucksbaum, M. Herzliner, S. D. Holmes, C. A. Lichtenstein, F. M. Pipkin, S. W. Raither and L. K. Siefertson, *Phys. Rev.* **D15** (1977) 594; C. J. Bebek, C. N. Brown, R. V. Kline, F. M. Pipkin, S. W. Raither, L. K. Hanson, D. Larson and A. Silverman, *Phys. Rev.* **D15** (1977) 3082;
- 5) P. Brauel, T. Canzler, D. Cords, R. Feist, G. Grindhammer, M. Helm, W. D. Kollmann, H. Krehbiel and M. Schadlich, *Phys Lett.* **B69** (1977) 253; P. Brauel, T. Canzler, D. Cords, R. Feist, G. Grindhammer, M. Helm, W. D. Kollmann, H. Krehbiel and M. Schadlich, *Z. Physik C, Particles and Fields* **3** (1979) 101;
- 6) O. Nachtmann, *Nucl. Phys.* **B74** (1974) 422;
- 7) R. Williams, private communications (1993);
- 8) J. W. Lightbody and J. S. O'Connell, *Comp. Phys.* May/June (1988) 57.

MODEL ZA ELEKTROTVORBU KAONA NA PROTONIMA I LAKIM  
JEZGRAMA

Posebno prikladan uređaj za proučavanje hadronske strukture je Pogon akceleratora za neprekidan elektronski snop (CEBAF) u S.A.D. zbog njegove snažne struje i točnosti. Za 1996. je odobreno mjerenje kojim treba odrediti omjer uzdužnih i poprečnih udarnih presjeka i utvrditi faktor oblika  $K^+$  putem reakcije  $p(e, e' K^+) \Lambda/\Sigma$ . Izračunali smo kinematičke uvjete i okidne modele za par okretnih spektrometara, s programom koji optimizira eksperimentalne uvjete, uzimajući u obzir očekivane udarne presjeke i prihvatnost (akceptancije) spektrometra.